ISSN 1070-3284, Russian Journal of Coordination Chemistry, 2018, Vol. 44, No. 2, pp. 138–146. © Pleiades Publishing, Ltd., 2018.
Original Russian Text © A.V. Piskunov, O.Yu. Trofimova, M.S. Piskunova, I.V. Smolyaninov, N.T. Berberova, G.K. Fukin, 2018, published in Koordinatsionnaya Khimiya, 2018, Vol. 44, No. 1, pp. 49–57.

Template Assembling of the Pentadentate Redox-Active Ligand in the Coordination Sphere of Tin(IV)

A. V. Piskunov[a, *], O. Yu. Trofimova[a], M. S. Piskunova[b], I. V. Smolyaninov[c, d], N. T. Berberova[d], and G. K. Fukin[a]

[a] *Razuvaev Institute of Organometallic Chemistry, Russian Academy of Sciences, ul. Tropinina 49, Nizhny Novgorod, 603950 Russia*
[b] *Nizhny Novgorod State Medical Academy, Nizhny Novgorod, Russia*
[c] *Astrakhan State Technical University, Astrakhan, Russia*
[d] *Southern Research Center, Russian Academy of Sciences, Rostov-on-Don, Russia*
**e-mail: pial@iomc.ras.ru*

Received July 11, 2017

Abstract—Heptacoordinated tin complexes with pentadentate redox-active ligands containing the diiminopyridine fragment combined with two sterically hindered phenolate coordination centers, LSnCl_2 and L'SnCl_2 (L and L' are dianions of deprotonated 2,6-bis[2,4-di-*tert*-butyl-6-(methylidenylamino)phenol]pyridine and 2,6-bis[2,4-di-*tert*-butyl-6-(ethylidenylamino)phenol]pyridine, respectively), are synthesized. The molecular and electronic structures of the synthesized compounds were studied by X-ray diffraction analysis (for complex **I**, CIF file CCDC no. 1557838), a set of spectral methods, and quantum-chemical calculations. The redox properties of the obtained complexes are characterized by cyclic voltammetry.

Keywords: template synthesis, tin(IV), X-ray diffraction analysis, cyclic voltammetry, redox-active ligands
DOI: 10.1134/S1070328418020082

INTRODUCTION

Schiff bases belong to one of the most universal classes of ligands for molecular design in the coordination chemistry of both transition and non-transition elements. The metal complexes with iminopyridine chelating ligands of this type are being studied actively for several decades [1]. The bi-, tri-, and tetradentate ligands are studied in most detail. At the same time, an increase in the denticity of chelating ligands favors the formation of more stable metal complexes due to providing a higher steric hindrance in the immediate vicinity of the central metal atom.

Tin complexes with redox-active ligands, such as *o*-quinones and their nitrogen-containing analogs, attract attention due to the specific structures and chemical properties of the obtained derivatives. The organotin derivatives of this type can be involved in reactions of oxidative addition and reductive elimination due to the redox-active ligand [2–7]. Increasing interest in these compounds is also caused by prospects of their use in various areas. For example, the *o*-quinone and *o*-iminoquinone tin derivatives act as chain growth regulators in the radical polymerization of the vinyl monomers [8–11]. In addition, the organotin derivatives are biologically active compounds and can be used as antimicrobial [12, 13], antifungal [14], bactericidal [15, 16], anti-inflammatory [17–19], and other drugs.

In this work, we studied the possibility of the synthesis of the tin(IV) complexes with the pentadentate redox-active ligands containing the diiminopyridine bridge linking two sterically hindered phenolate fragments (Scheme 1). Chelating pentadentate ligands of this type are poorly studied. The zinc [20, 21], cadmium [22], tin [23], manganese [24], rhenium [25], and cobalt [26] compounds based on these ligands are known at the moment.

Six various redox states are theoretically possible for the above indicated pentadentate ligands (Scheme 1). The dianionic (L^2) and tetraanionic (L^4) species are diamagnetic, whereas the mono- (L^1), tri- (L^3), and pentaanionic (L^5) species are paramagnetic. The neutral ligand (L^0) should be biradical in nature.

All metal complexes known at the moment contain the dianionic form of this type of ligands [20–26], and no attempts to carry out their redox transformations were made.

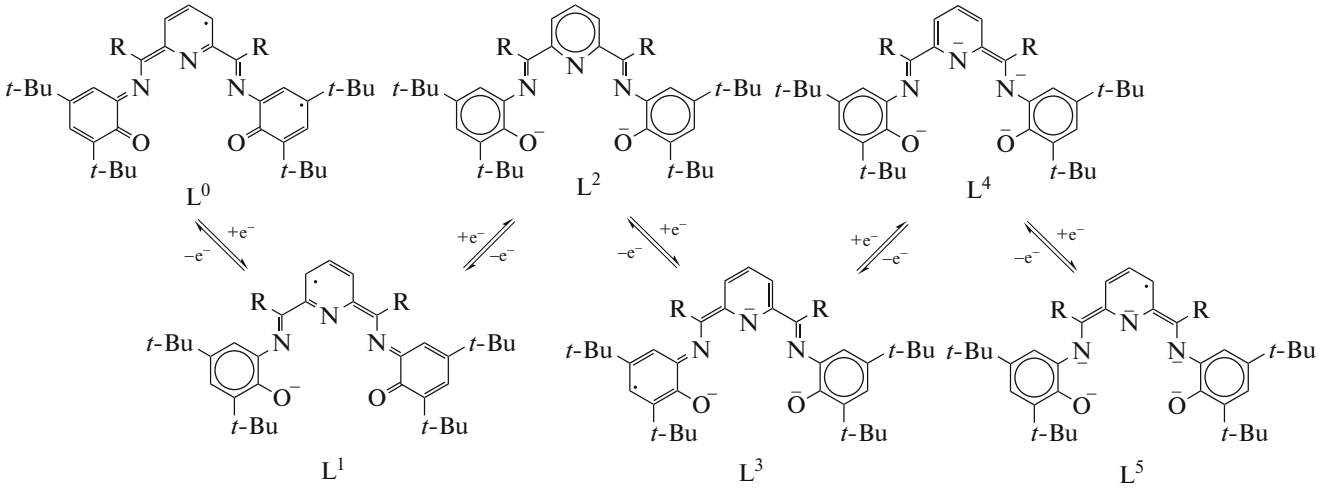

Scheme 1

EXPERIMENTAL

IR spectra were recorded on an FSM-1201 FT-IR spectrometer in a range of 4000–400 cm^{-1} in Nujol (KBr cells). NMR spectra were detected on a Bruker Avance III spectrometer (400 MHz) in $CDCl_3$ using Me_4Si as an internal standard. Electronic absorption spectra were recorded on a UV-3600 UV-VIS-NIR spectrophotometer (SHIMADZU).

Electrochemical potentials of the studied compounds were measured by cyclic voltammetry (CV) in a three-electrode curve using an IPC-pro potentiostat in CH_2Cl_2 in an argon atmosphere. A stationary glassy carbon (GC) electrode with a diameter of 2 mm served as a working electrode. A platinum wire ($S = 18$ mm^2) was used as an auxiliary electrode. The reference electrode (Ag/AgCl/KCl) with the water-proof membrane was used. The concentration of the studied compounds was 0.002–0.003 mol/L. The number of electrons transferred in the course of the electrode process was estimated relative to the standard (ferrocene). The potential scan was 0.2 V/s. The supporting electrolyte was 0.1 M Bu_4NClO_4 (99%, Acros) doubly recrystallized from aqueous EtOH and dried in vacuo (48 h) at 50°C.

The following commercial reagents were used: pyridine-2,6-dimethanol, 2,6-diacetylpyridine, and tin(IV) chloride. Pyridine-2,6-dicarboxaldehyde [27] and 2-amino-4,6-di-*tert*-butylphenol [28] were synthesized according to known procedures.

All procedures on the synthesis of the tin complexes were carried out under aerobic conditions. The solvents used (reagent grade and analytical grade) were dried according to standard procedures [29].

The quantum-chemical calculations for the $LSnCl_2$ complex (L is dianion of deprotonated 2,6-bis[2,4-di-*tert*-butyl-6-(methylidenylamino)phenol]pyridine (**I**) were performed using the Gaussian 09 program [30] by the density functional theory (DFT) in terms of the B3LYP functional [31] with the full-electron DGDZVP basis set for all atoms. The absence of imaginary frequencies indicates that the optimized molecule is at the potential energy minimum.

Synthesis of complex I. Pyridine-2,6-dicarboxaldehyde (1 mmol, 0.135 g), 2-amino-4,6-di-*tert*-butylphenol (2 mmol, 0.442 g), and $SnCl_4$ (1 mmol, 0.261 g) were mixed in a solution of methanol (20 mL). The subsequent heating of the reaction mixture to boiling was accompanied by the appearance of an intense violet color and the precipitation of dark violet complex **I**. The precipitate was collected on the Schott

filter and washed with methanol (5 mL). The yield was 0.525 g (72%).

For $C_{35}H_{45}N_3O_2Cl_2Sn$

Anal. calcd., %	C, 57.64	H, 6.22	N, 5.76
	Cl, 9.72	Sn, 16.28	
Found, %	C, 57.66	H, 6.17	N, 5.80
	Cl, 9.74	Sn, 16.24	

IR (Nujol), ν, cm^{-1}: 1604 s, 1516 s, 1471 s, 1361 s, 1263 s, 1201 s, 1167 s, 857 s, 830 s, 772 s.

^1H NMR ($CDCl_3$, 293 K), δ, ppm: 1.31 (s, 18 H, *t*-Bu), 1.52 (s, 18 H, *t*-Bu), 7.23 (s, 2 H, H_{arom}), 7.42 (s, 2 H, H_{arom}), 7.68 (d, 2 H, J = 7.3 Hz, H_{Py}), 8.09 (t, 1 H, J = 7.3 Hz, H_{Py}), 8.50 (s, 2 H, J ($^{119}Sn-^1H$) = 72.9 Hz, CH). ^{13}C NMR ($CDCl_3$), δ, ppm: 29.14, 31.17 (CH_3(*t*-Bu)), 34.48, 35.58 (C(*t*-Bu)), 109.90, 124.39, 125.97, 130.34, 132.19, 139.19, 141.11, 142.50, 143.77 (C_{arom}), 159.32 (C=N, J ($^{119}Sn-^{13}C$) = 72.9 Hz). ^{119}Sn NMR ($CDCl_3$, 293 K), δ, ppm: −673.48.

The crystals of complex **I** for X-ray diffraction analysis were obtained by slow crystallization from a CH_2Cl_2–toluene (1 : 1) solution.

Synthesis of complex L'$SnCl_2$ (L' is dianion of deprotonated 2,6-bis[2,4-di-*tert*-butyl-6-(ethylidenylamino)phenol]pyridine (**II**). 2,6-Diacetylpyridine (1 mmol, 0.163 g), 2-amino-4,6-di-*tert*-butylphenol (2 mmol, 0.442 g), and $SnCl_4$ (1 mmol, 0.261 g) were mixed in a solution of methanol (20 mL) at 65°C. The reaction mixture was stirred for 30 min to the formation of a dark violet precipitate. The obtained product was collected on the Schott filter and washed with methanol (5 mL). The yield was 0.515 g (68%).

For $C_{37}H_{49}N_3O_2Cl_2Sn$

Anal. calcd., %	C, 58.67	H, 6.52	N, 5.55
	Cl, 9.36	Sn, 15.67	
Found, %	C, 58.68	H, 6.48	N, 5.57
	Cl, 9.40	Sn, 15.69	

IR (Nujol), ν, cm^{-1}: 1596 s, 1522 s, 1443 s, 1361 s, 1264 s, 1204 s, 1174 s, 842 s, 828 s, 777 s.

^1H NMR ($CDCl_3$, 293 K), δ, ppm: 1.32 (s, 18H, *t*-Bu), 1.57 (s, 18H, *t*-Bu), 2.92 (s, 6 H, J ($^{119}Sn-^1H$) = 130.1 Hz, CH_3), 7.27 (d, 2 H, J = 1.8 Hz, H_{arom}), 7.43 (d, 2 H, J = 1.8 Hz, H_{arom}), 7.95–8.00 (m, 2 H, H_{Py}), 8.19 (t, 1 H, J = 7.8 Hz, H_{Py}). ^{13}C NMR ($CDCl_3$), δ, ppm: 18.4 (CH_3, J ($^{119}Sn-^{13}C$) = 17.6 Hz), 29.47, 31.42 (CH_3(*t*-Bu)), 34.38, 35.66 (C(*t*-Bu)), 116.1 (J ($^{119}Sn-^{13}C$) = 29.9 Hz), 123.8 (J ($^{119}Sn-^{13}C$) = 10.2 Hz), 125.8 (J ($^{119}Sn-^{13}C$) = 105.85 Hz), 128.1, 137.5, 139.7 (J ($^{119}Sn-^{13}C$) = 56.9 Hz), 143.2, 145.6 (J ($^{119}Sn-^{13}C$) = 44.8 Hz), 146.4 (J ($^{119}Sn-^{13}C$) = 27.2 Hz) (C_{arom}), 158.6 (C=N, J ($^{119}Sn-^{13}C$) = 32.4 Hz). ^{119}Sn NMR ($CDCl_3$, 293 K), δ, ppm: −667.11.

The X-ray diffraction analysis of complex **I** was carried out on a Bruker D8 Quest diffractometer at 100 K (λ(MoK_α) = 0.71073 Å). The structure of the compound were solved by direct methods and refined by least squares for F^2 in the full-matrix anisotropic approximation for all non-hydrogen atoms (SHELXTL) [32]. An absorption correction was applied by the SADABS program [33].

The total number of measured reflections was 43240 of which 8698 (R_{int} = 0.0271) were independent with $I > 2\sigma(I)$. The crystals were orthorhombic, at 100(2) K: a = 12.2616(8), b = 17.9749(12), c = 18.1890(12) Å, space group $P2_12_12_1$, Z = 4, V = 4008.9(5) $Å^3$, ρ_{calc} = 1.361 g/cm^3, μ = 0.809 mm^{-1}, 2.51° ≤ θ ≤ 27.00°, R_1 = 0.0268, wR_2 = 0.0715 ($I > 2\sigma(I)$), R_1 = 0.0286, wR_2 = 0.0727 (for all data), $S(F^2)$ = 0.998.

The crystallographic data were deposited with the Cambridge Crystallographic Data Centre (CIF file CCDC no. 1557838; deposit@ccdc.cam.ac.uk or http://www.ccdc.cam.ac.uk/data_request/cif).

RESULTS AND DISCUSSION

The first attempts to synthesize a cobalt complex based on the pentadentate ligand (L) (R = H) were made in [26]. The reaction of the doubly protonated form L^2H_2 with cobalt(II) acetate in acetonitrile affords an unstable metal complex in a yield of ~40%, and the composition of the complex corresponds to the formula [$L^2Co(H_2O)_2$]. The compound obtained decomposes rapidly in a solution accompanied by the oxidative cyclization of ligand L [26]. We applied another approach to the synthesis of tin complexes of a similar type. The heptacoordinated tin(IV) complexes with the pentadentate redox-active ligands were obtained by template synthesis with the simultaneous heating of pyridine-2,6-dicarboxaldehyde (2,6-diacetylpyridine), 2-amino-4,6-di-*tert*-butylphenol, and tin(IV) chloride in a methanol solution (Scheme 2). The reaction mixture instantly turned intensely violet in the course of the reaction. The reaction ceases within 30 min, and complexes **I** and **II** formed are isolated in the analytically pure form as finely crystalline dark violet precipitates. The synthesized compounds are resistant to air oxygen and moisture in both the crystalline state and solution.

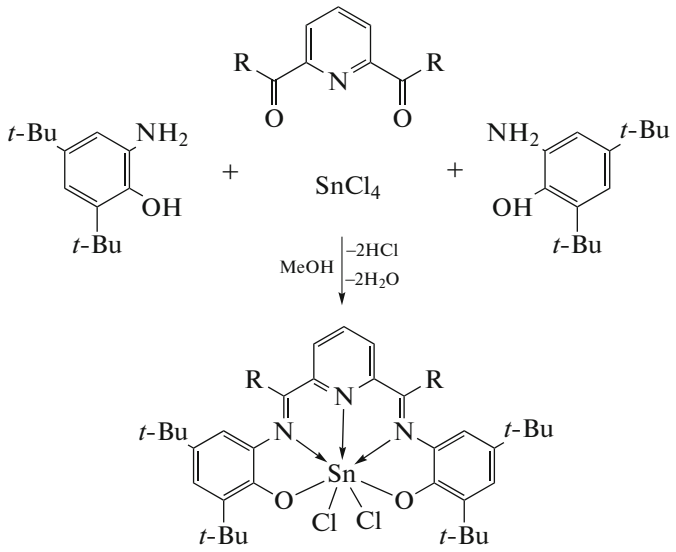

R = H (**I**), Me (**II**)

Scheme 2

The compositions and structures of the synthesized compounds were determined by IR spectroscopy, NMR spectroscopy, electronic absorption spectroscopy, and elemental analysis. The X-ray diffraction analysis was carried out for complex **I**.

The IR spectra of complexes **I** and **II** exhibit intense absorption bands in ranges of 1700–1500 and 1300–1000 cm^{-1} characteristic of double C=N [29] and ordinary C–N and C–O [29] bonds, respectively.

The heptacoordinated environment of tin is characterized by the upfield shift of the signal in the ^{119}Sn NMR spectrum, which is consistent with the previous studies [34, 35]. The resonance is observed at –673 and –667 ppm for compounds **I** and **II**, respectively. It is interesting that the ^{119}Sn NMR spectra of the tin compounds with pentadentate ligands of similar structure and containing alkyl (aryl) substituents at the metal atom exhibit a signal in the range from –370 to –404 ppm [22]. This difference in the peak positions for the heptacoordinated tin complexes is explained by the influence of the electronegativity of the substituents on the electron density distribution around the metal atom. The signal in the ^{119}Sn NMR spectrum undergoes an upfield shift under the action of the electron-withdrawing substituents (Cl) in complexes **I** and **II**, whereas the shift is downfield in the case of the electron-donating hydrocarbon substituents [22].

The molecular structure of complex **I** is shown in Fig. 1. The values of selected bond lengths and bond angles are given in Table 1. The crystalline cell contains one solvate molecule of toluene based on one molecule of the complex. The tin atom is coordinated at the vertices of a distorted pentagonal bipyramid. The equatorial plane is formed by the chelating atoms of the organic ligand O(1), O(2), N(1), N(2), and N(3), and the apical positions are occupied by the Cl(1) and Cl(2) atoms (the ClSnCl angle is 168.97(2)°). The values of the Sn(1)–O(1) and Sn(1)–O(2) bond lengths (2.049(2) and 2.0640(19) Å) are smaller than the sum of the covalent radii of Sn and O (2.11 Å) [36]. The Sn(1)–N(1), Sn(1)–N(2), and Sn(1)–N(3) distances (2.292(2), 2.294(2), and 2.316(2) Å) substantially exceed the sum of the covalent radii of the metal and nitrogen (2.12 Å) [36] but are smaller then the sum of the van der Waals radii of the corresponding elements (3.8 Å) [36], which corresponds to coordination bonding. The bond length distribution in the phenolate fragments of the organic ligand differs substantially from that in the known amido- and aminophenolate ligands [37]. A distortion of the quinoid type is observed in the C(1)–C(6) and C(14)–C(19) aromatic rings. The C(3)–C(4) and C(5)–C(6) bonds are appreciably shorter than C(1)–C(2), C(2)–C(3), C(4)–C(5), and C(1)–C(6). The O(1)–C(2) and O(2)–C(15) bond lengths (1.315(3) and 1.313(3) Å) are also more close to the values observed in the *o*-semiquinone [38, 39] and *o*-iminosemiquinone [4, 40] tin complexes that those in the

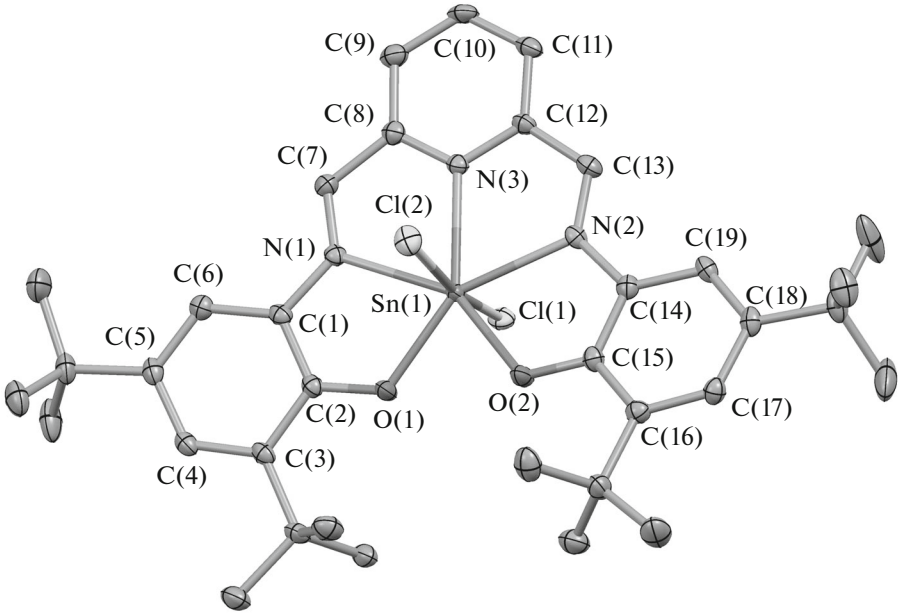

Fig. 1. Molecular structure in complex **I**. Thermal ellipsoids are presented with 50% probability. Hydrogen atoms are omitted for clarity.

amidophenolate and catecholate tin complexes [2–6]. A similar bond length distribution has been observed previously in the tin(IV) complexes based on the tetradentate ligand containing two similar phenolate fragments linked by the diimine bridge [41]. The intraligand charge transfer from the anionic phenolate groups to the diiminopyridine fragment resulted in the above described change in the bond lengths and is accompanied by the appearance of an intense absorption in the long-wavelength range of the electronic absorption spectra of compounds **I** and **II** (Fig. 2).

The electronic structure of compound **I** was studied by the DFT quantum-chemical calculations, according to which the frontier orbitals responsible for the redox behavior of the complex have the pronounced ligand nature. In complex **I**, the highest occupied molecular orbital (HOMO, –5.57 eV) is localized on the donor phenolate fragments of the organic ligand, whereas the lowest unoccupied molecular orbital (LUMO, –3.29 eV) is localized on the acceptor diiminopyridine fragment (Fig. 3). The energy gap width between the frontier orbital (LUMO–HOMO) in compound **I** determines the position of the long-wavelength peak in the electronic absorption spectrum and is equal to 2.28 eV. The obtained value is consistent with the data of electronic absorption spectroscopy: $\Delta E = 2.08$ eV ($\lambda = 598$ nm).

The electrochemical properties of complexes **I** and **II** were studied by the CV method in a dichloromethane solution at the GC electrode. The electrochemical reduction of complex **I** proceeds in three consecutive steps. The first one-electron redox transition is irreversible, and the subsequent two cathodic steps are quasi-reversible (Fig. 4a). The irreversible character of the first step indicates that the fast chemical reaction occurs in the solution. For the formed primary intermediate, the iminopyridine fragment is also involved in the electron density delocalization, and the protonation of this fragment can results in the loss of reversibility of the first redox transition (Scheme 3).

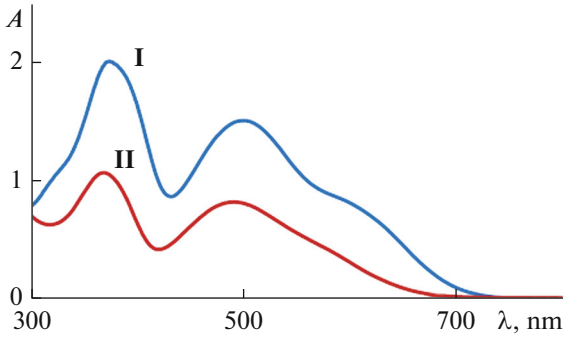

Fig. 2. Absorption spectra of complexes **I** and **II** in THF ($T = 295$ K, $c = 1 \times 10^{-4}$ mol/L, $L = 1$ cm). Complex **I** (λ, nm (ε, l cm^{-1} mol^{-1})): 368 (19569), 498 (15037), 598 (8195); complex **II** (λ, nm (ε, l cm^{-1} mol^{-1})): 361 (10207), 484 (8009).

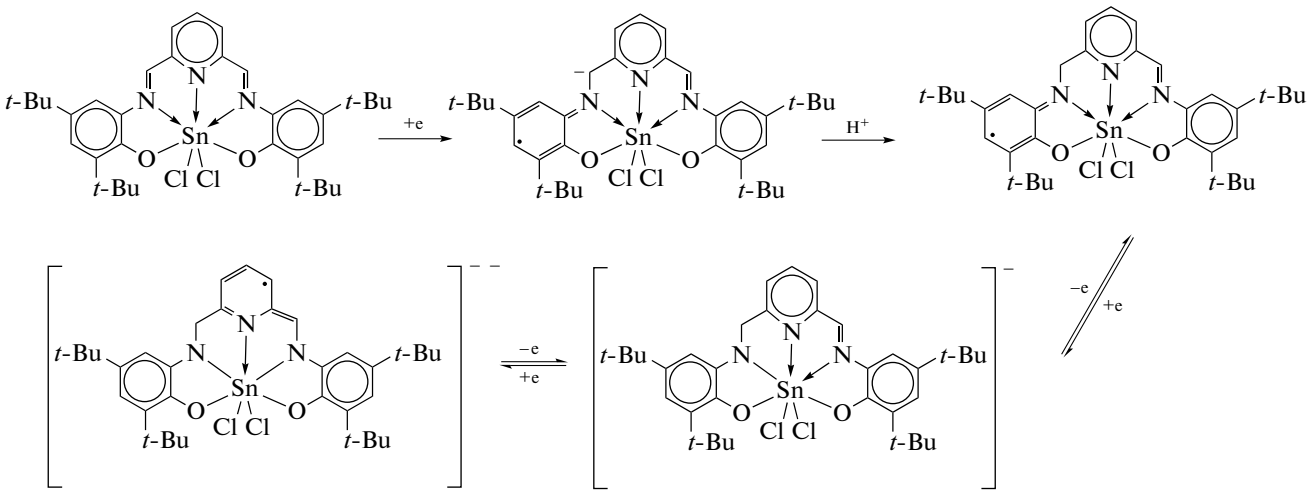

Scheme 3

Table 1. Selected bond lengths and bond angles in complex **I**

Bond	*d*, Å	Bond	*d*, Å
Sn(1)–O(1)	2.049(2)	C(2)–C(3)	1.421(4)
Sn(1)–O(2)	2.0640(19)	C(3)–C(4)	1.376(4)
Sn(1)–N(2)	2.292(2)	C(4)–C(5)	1.413(4)
Sn(1)–N(3)	2.294(2)	C(5)–C(6)	1.369(4)
Sn(1)–N(1)	2.316(2)	C(7)–C(8)	1.455(4)
Sn(1)–Cl(2)	2.3884(7)	C(8)–C(9)	1.395(4)
Sn(1)–Cl(1)	2.4090(7)	C(9)–C(10)	1.382(4)
O(1)–C(2)	1.315(3)	C(10)–C(11)	1.383(4)
O(2)–C(15)	1.313(3)	C(11)–C(12)	1.390(4)
N(1)–C(7)	1.285(4)	C(12)–C(13)	1.458(4)
N(1)–C(1)	1.382(4)	C(14)–C(15)	1.406(4)
N(2)–C(13)	1.286(4)	C(14)–C(19)	1.414(4)
N(2)–C(14)	1.383(4)	C(15)–C(16)	1.429(4)
N(3)–C(12)	1.333(4)	C(16)–C(17)	1.385(4)
N(3)–C(8)	1.336(4)	C(17)–C(18)	1.405(4)
C(1)–C(6)	1.396(4)	C(18)–C(19)	1.374(4)
C(1)–C(2)	1.410(4)		
Angle	ω, deg	Angle	ω, deg
O(1)Sn(1)O(2)	76.01(8)	N(2)Sn(1)Cl(2)	91.20(6)
O(1)Sn(1)N(2)	148.83(8)	N(3)Sn(1)Cl(2)	86.01(6)
O(2)Sn(1)N(2)	73.61(8)	N(1)Sn(1)Cl(2)	86.11(6)
O(1)Sn(1)N(3)	141.28(8)	O(1)Sn(1)Cl(1)	91.30(6)
O(2)Sn(1)N(3)	142.64(8)	O(2)Sn(1)Cl(1)	96.83(6)
N(2)Sn(1)N(3)	69.12(9)	N(2)Sn(1)Cl(1)	85.55(6)
O(1)Sn(1)N(1)	73.12(8)	N(3)Sn(1)Cl(1)	82.98(6)
O(2)Sn(1)N(1)	148.66(8)	N(1)Sn(1)Cl(1)	89.20(6)
O(1)Sn(1)Cl(2)	96.87(6)	Cl(2)Sn(1)Cl(1)	168.97(2)
O(2)Sn(1)Cl(2)	92.35(6)		

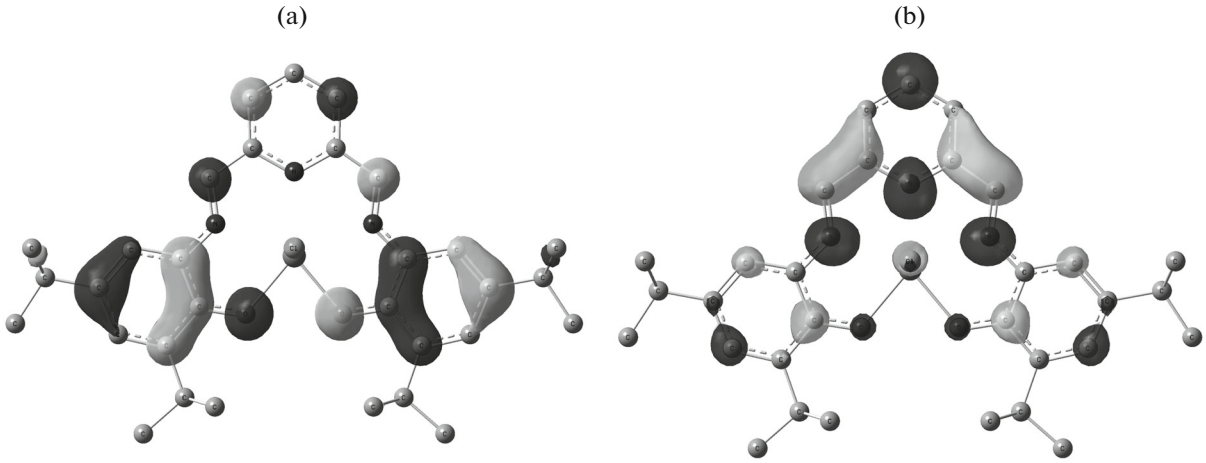

Fig. 3. Frontier orbitals of the (a) HOMO and (b) LUMO for complex **I**.

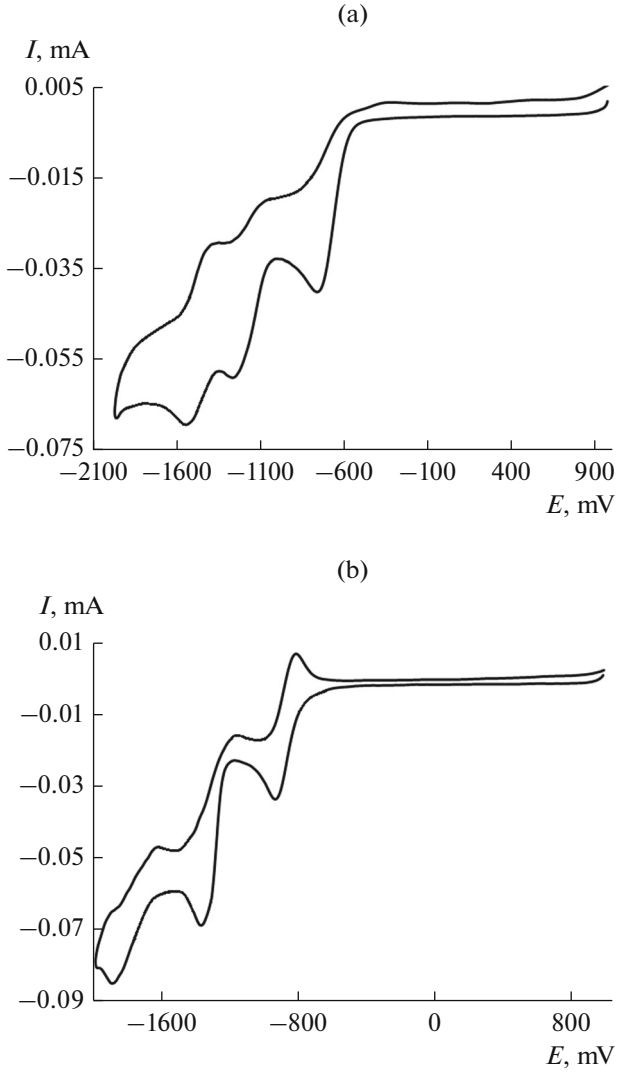

Fig. 4. Cyclic voltammetry of the reduction of complexes (a) **I** and (b) **II** (CH_2Cl_2, GC anode, Ag/AgCl/KCl, 0.1 M NBu_4ClO_4, $c = 3 \times 10^{-3}$ mol/L, argon).

Unlike compound **I**, complex **II** is characterized by the reversible one-electron transfer in the first step of reduction (Fig. 4b). According to Scheme 1, the ligand in the L^2 form is transformed into the radical form L^3 due to the transfer of one electron. In the case of complex **II**, the shielding methyl group in this fragment of the ligand favors the stabilization of the reduced form and prevents the protonation by moisture traces in the solvent, which results, correspondingly, in the fixation of the reversible redox transition.

The subsequent electrochemical reduction (Scheme 3) of complex **I** leads to the generation of the poorly stable mono- and dianions, which confirms a low reversibility coefficient of the second cathodic process (Table 2) and a decrease in the number of transferred electrons ($n < 1$) involved in the third step. Similar changes can be due to the decoordination of the halide ligands bound to the tin(IV) atom.

The introduction of methyl groups into the iminopyridine fragment of the ligand shifts the reduction potentials of complex **II** to the cathodic region compared to compound **I**. The second cathodic process is also quasi-reversible, but the number of electrons involved in the electrode reaction exceeds the one-electron level. Two reduction steps are joined into one cathodic process. In the region of higher cathodic potentials, an additional redox process is observed at a peak potential of −1.89 V, which characterizes the further reduction of the redox-active ligand.

The electrooxidation of complexes **I** and **II** proceeds identically (Fig. 5). The first one-electron redox transition is quasi-reversible and characterizes the formation of the radical cation intermediate containing the ligand in the L^1 form and stable within the time of the CV experiment. Two electrons are transferred in the second quasi-reversible anodic step, which is

Table 2. Electrochemical parameters of complexes **I** and **II** ($c = 3 \times 10^{-3}$ mol/L, argon, 0.1 M NBu_4ClO_4, $V = 0.2$ V/s, vs. Ag/AgCl (sat.)*

Compound	$E_{1/2}^{red1}$, V	I_a/I_c	$E_{1/2}^{red2}$, V	I_a/I_c	$E_{1/2}^{red3}$, V	$E_{1/2}^{ox1}$, V	I_c/I_a	$E_{1/2}^{ox2}$, V
I	−0.76**		−1.13	0.4	−1.45	1.19	0.8	1.49
II	−0.87	0.8	−1.28	0.6	−1.89*	1.17	1.0	1.49

* $E_{1/2}^{red}$ is the half-wave potential of the cathodic process, $E_{1/2}^{ox}$ is the half-wave potential of the anodic process, I_a/I_c is the ratio of peak currents of the direct and reverse potential scans (reversibility coefficient).

** Potential of the irreversible cathodic peak (E_{pc1}).

related to the close oxidation potentials of the phenolate fragment and imino group in *o*-iminobenzoquinones [42]. The oxidation of two redox-active moieties of the molecule results in further chemical transformations in the solution accompanied by the formation of the reaction products detected at the reverse branch of the CV curve at the potential scan to 1.80 V (Fig. 6, *1*). The values of reversibility coefficients (Table 2) indicate that the oxidized monocationic form of complex **II** is more stable than a similar species for compound **I**. The values obtained for redox potentials of the studied complexes also make it possible to calculate the energy gap width between the frontier redox orbitals: 2.04 eV for compound **II** and 2.00 eV for compound **I**. The obtained values are consistent with the results of electronic absorption spectroscopy.

Thus, a prospect for using the template assembling method was demonstrated for the targeted design of the metal complexes with the Schiff bases containing the diiminopyridine fragment. The new heptacoordinated tin(IV) complexes based on the pentadentate redox-active ligands were obtained by the one-pot synthesis. The redox properties of the synthesized compounds were studied using cyclic voltammetry. The introduction of methyl substituents to the imine carbon atoms significantly increases the stability of the one-electron oxidation and reduction products.

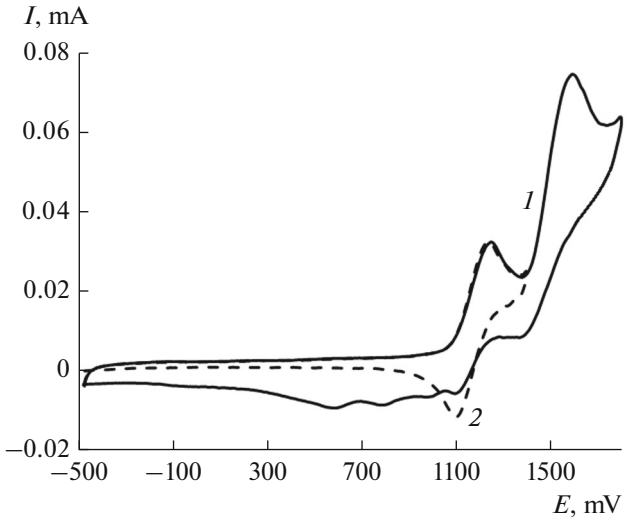

Fig. 5. Cyclic voltammetry of the oxidation of complex **II** at the potential scan (*1*) from −0.48 to 1.80 V and (*2*) from −0.48 to 1.40 V; CH_2Cl_2, GC anode, Ag/AgCl/KCl, 0.1 M NBu_4ClO_4, $c = 3 \times 10^{-3}$ mol/L, argon).

ACKNOWLEDGMENTS

This work was supported by the Council on Grants of the President of the Russian Federation (projects nos. MK-5285.2016.3 and NSh-7916.2016.3).

REFERENCES

1. Hernandez-Molina, R. and Mederos, A., in *Comprehens. Coord. Chem. II*, Lever, A.B.P., Ed., Elsevier, 2004.
2. Lado, A.V., Piskunov, A.V., Cherkasov, V.K., et al., *Russ. J. Coord. Chem.*, 2006, vol. 32, no. 3, p. 173.
3. Piskunov, A.V., Mescheryakova, I.N., Fukin, G.K., et al., *Chem.-Eur. J.*, 2008, vol. 14, p. 10085.
4. Piskunov, A.V., Chegerev, M.G., Vaganova, L.B., and Fukin, G.K., *Russ. J. Coord. Chem.*, 2015, vol. 41, no. 7, p. 428.
5. Piskunov, A.V., Chegerev, M.G., and Fukin, G.K., *J. Organomet. Chem.*, 2016, vol. 803, p. 51.
6. Chegerev, M.G., Piskunov, A.V., Maleeva, A.V., et al., *Eur. J. Inorg. Chem.*, 2016, p. 3813.
7. Piskunov, A.V., Piskunova, M.S., and Chegerev, M.G., *Izv. Akad. Nauk, Ser. Khim.*, 2014, p. 912.
8. Kolyakina, E.V., Vaganova, L.B., Lado, A.V., et al., *Izv. Akad. Nauk, Ser. khim.*, 2007, p. 1314.
9. Vaganova, L.B., Maleeva, A.V., Piskunov, A.V., and Grishin, D.F., *Izv. Akad. Nauk, Ser. Khim.*, 2015, p. 346.
10. Vaganova, L.B., Shchepalov, A.A., Meshcheryakova, I.N., et al., *Dokl. Akad. Nauk*, 2012, vol. 447, p. 634.
11. Vaganova, L.B., Kaprinina, A.N., Meshcheryakova, I.N., et al., *Izv. Akad. Nauk, Ser. Khim.*, 2014, p. 744.
12. Shahzadi, S., Ali, S., Bhatti, M.H., et al., *J. Organomet. Chem.*, 2006, vol. 691, p. 1797.
13. Girasolo, M.A., Schillaci, D., Di Salvo, C., et al., *J. Organomet. Chem.*, 2006, vol. 691, p. 693.
14. Khan, M.I., Baloch, M.K., and Ashfaq, M., *J. Organomet. Chem.*, 2004, vol. 689, p. 3370.

15. Din Molloy, K.C. Mazhar, M., et al., *Appl. Organomet. Chem.*, 2003, vol. 17, p. 781.
16. Casas, J.S., García Martínez, E., Jorge, M.L., et al., *Appl. Organomet. Chem.*, 2002, vol. 15, p. 204.
17. Nath, M., Pokharia, S., Eng, G., et al., *J. Organomet. Chem.*, 2003, vol. 669, p. 109.
18. Nath, M., Pokkaria, S., Eng, G., et al. *Synth. React. Inorg. Metal-Org. Chem.*, 2004, vol. 34, p. 1689.
19. Kovala-Demertzi, D., *J. Organomet. Chem.*, 2006, vol. 691, p. 1767.
20. Sun, X.-X., Qi, C.-M., Ma, S.L., et al., *Inorg. Chem. Commun.*, 2006, vol. 9, p. 911.
21. Janssen, F.F.B.J., Peters, L.C.J.M., Schlebos, P.P.J., et al., *Inorg. Chem.*, 2013, vol. 52, p. 13004.
22. Liles, D.C., McPartlin, M., Tasker, P.A., et al., *J. Chem. Soc., Chem. Commun.*, 1976, p. 549.
23. Gonzalez, A., Gomez, E., Cortes-Lozada, A., et al., *Chem. Pharm. Bull.*, 2009, vol. 57, p. 5.
24. Kampert, E., Janssen, F.F.B.J., Boukhvalov, D.W., et al., *Inorg. Chem.*, 2009, vol. 48, p. 11903.
25. Potgieter, K., Mayer, P., Gerber, T.I.A., and Booysen, I.N., *Polyhedron*, 2009, vol. 28, p. 2808.
26. Garza-Ortiz, A., Martinez, P.A., Duarte-Hernandez, A.M., et al., *J. Mol. Struct.*, 2013, vol. 30, p. 265.
27. Papadopoulos, E.P., Jarrar, A., and Issidorides, C.H., *Org. Chem.*, 1966, vol. 31, p. 615.
28. Vol'eva, V.B., Prokof'eva, T.I., Prokof'ev, A.I., et al., *Izv. Akad. Nauk, Ser. Khim.,* 1995, p. 1789.
29. Gordon, A. and Ford, R., *The Chemist's Companion: A Handbook of Practical Data, Techniques, and References*, New York: Wiley, 1972.
30. Frisch, M.J., Trucks, G.W., Schlegel, H.B., et al., *Gaussian 09. Revision D.01*, Wallingford: Gaussian, Inc., 2013.
31. Becke, A.D., *J. Chem. Phys.*, 1986, vol. 84, p. 4524.
32. Sheldrick, G.M., *SHELXTL. Version 6.12. Structure Determination Software Suite*, Madison: Bruker AXS, 2000.
33. Sheldrick, G.M., *SADABS. Version 2.01. Bruker/Siemens Area Detector Absorption Correction Program*, Madison: Bruker AXS, 1998.
34. Wrackmeyer, B., *Annu. Rep. NMR Spectrosc.*, 1985, vol. 16, p. 73.
35. Wrackmeyer, B., *Annu. Rep. NMR Spectrosc.*, 1999, vol. 38, p. 203.
36. Batsanov, S.S., *Zh. Neorg. Khim.*, 1991, vol. 36, p. 3015.
37. Poddels'ky, A.I., Cherkasov, V.K., and Abakumov, G.A., *Coord. Chem. Rev.*, 2009, vol. 253, p. 291.
38. Abakumov, G.A., Cherkasov, V.K., Piskunov, A.V., et al., *Dokl. Akad. Nauk*, 2006, vol. 410, p. 57.
39. Ilyakina, E.V., Poddel'sky, A.I., Piskunov, A.V., et al., *Inorg. Chim. Acta*, 2013, vol. 394, p. 282.
40. Piskunov, A.V., Meshcheryakova, I.N., Baranov, E.V., et al., *Izv. Akad. Nauk, Ser. Khim.* 2010, p. 354.
41. Piskunov, A.V., Trofimova, O.Yu., Fukin, G.K., et al., *Dalton Trans.*, 2012, vol. 41, p. 10970.
42. Smolyaninov, I.V., Letichevskaya, N.N., Kulakov, A.V., et al., *Elektrokhimiya*, 2007, vol. 43, p. 1251.

Translated by E. Yablonskaya